

Article

Improved H₂ Production by Ethanol Steam Reforming over Sc₂O₃-Doped Co-ZnO Catalysts

Xuelian Liang, Xinping Shi, Fanfan Zhang, Yuyang Li, Hongbin Zhang and Youzhu Yuan * 

Department of Chemistry, College of Chemistry and Chemical Engineering, State Key Laboratory of Physical Chemistry for Solid Surfaces and National Engineering Laboratory for Green Chemical Productions of Alcohols-Ethers-Esters, Xiamen University, Xiamen 361005, Fujian, China; xliang@xmu.edu.cn (X.L.); 20520141151591@stu.xmu.edu.cn (X.S.); 20620151152252@stu.xmu.edu.cn (F.Z.); 20620151152208@stu.xmu.edu.cn (Y.L.); hbzhang@xmu.edu.cn (H.Z.)

* Correspondence: yzyuan@xmu.edu.cn; Tel.: +86-592-2181659

Received: 2 July 2017; Accepted: 16 August 2017; Published: 18 August 2017

Abstract: H₂ production by catalytically ethanol steam reforming (ESR) is an effective and prospective method for the application of fuel cells. However, the catalysts' desirable activity and stability remains an unprecedented challenge. Herein, a type of Sc₂O₃-doped Co-ZnO catalyst was developed by a co-precipitation method. The so-constructed Co₂Zn₁Sc_{0.3} catalyst exhibited a superb catalytic performance compared with Co-ZnO, giving a STY(H₂) as high as 1.099 mol·h⁻¹·g_{cat}⁻¹ (data taken 100 h after the reaction started). In comparison, the pristine Co-ZnO catalyst only afforded a STY(H₂) of 0.684 mol·h⁻¹·g_{cat}⁻¹ under identical reaction conditions. Characterization results revealed that the Sc₂O₃ dopant strengthened the electronic interaction between Co species and ZnO, which was in favour of elevating the reduction temperature of Co oxides and boosting the dispersion of the Coⁿ⁺ (*n* = 1 or 2). The introduction of Sc₂O₃ induced the formation of O²⁻ and OH⁻. All of these effects effectively inhibited the sintering of active Co species and markedly improved the activity and operating stability of the catalyst.

Keywords: Co-ZnO catalyst; Sc₂O₃; doping; ethanol steam reforming; H₂ production

1. Introduction

Ethanol is an important candidate as a chemical carrier of hydrogen for fuel cell applications. Not only is it less hazardous than methanol, it can be also produced from a variety of biomass sources. Therefore, much attention is recently focused on the development of suitable catalysts for steam reforming of ethanol (ESR; C₂H₅OH + 3H₂O → 2CO₂ + 6H₂) [1,2]. A number of reported catalysts have demonstrated good performance in terms of activity and selectivity for the ethanol steam reforming (ESR) reaction, i.e., Rh (or Pt or Pd)/CeO₂-ZrO₂ [3,4], Ni-Rh/CeO₂ [5], Ir/CeO₂ [6], Pt/CeZrO₂ [7], Co/ZnO [8,9], Co/Al₂O₃ (/SiO₂ or /MgO) [10], Co/ZrO₂ (or /CeO₂) [11–13], Pt-Co/ZnO [14], Ni/Y₂O₃ (or /ZrO₂) [15–17], Ni/Mg-Al mixed oxide [18,19], and Ni/ZrO₂-Yb₂O₃ [20]. Although noble metal-based catalysts showed excellent catalytic activities for ESR, their application on a large scale was limited due to scarcity and expense.

In this regard, the development of non-precious metal-based catalysts is imperative for chemists. ZnO possesses the eminent catalytic reactivity of ESR. The incorporation of Co to ZnO apparently improves its performance [21], and the low cost and excellent performance of the Co-ZnO catalyst has attracted considerable attention and been widely reported. However, although some promising results have been obtained on the ESR reaction, there are still several problems to be solved, such as low stability and high reaction temperature. The results of Song et al. [11,12] indicated that the catalyst deactivation was due to the carbon deposition and cobalt sintering. Introduction of ceria improved activity and durability because of the higher oxygen mobility of ceria. The addition of sodium

could evidently enhance the catalytic performance of Co-ZnO, which was attributed to reduction in coke formation [9]. In addition, the reactivity of Co-ZnO catalysts could be further increased by impregnation of Pt [14].

Based on the aforementioned summarization, catalyst stability is one of the most crucial challenges in the development of catalysts for producing hydrogen from ESR. Catalyst deactivation is generally attributed to the carbon deposition, sintering, and oxidation of metal particles [1,13,22–27]. Carbon deposition in the form of filaments or whiskers is often found in addition to amorphous carbon.

It is well known that the radius of Sc^{3+} (0.073 nm) is close to that of Zn^{2+} (0.074 nm). Thus, Sc_2O_3 may be readily embedded into the ZnO crystal lattice by ion-doped method in order to modify the crystal structure of ZnO and achieve more stable composites. With these ideas in mind, a series of Sc_2O_3 -doped Co-ZnO catalysts were prepared. The physicochemical properties of the catalysts were examined by Transmission electron microscopy (TEM), X-ray Powder Diffraction (XRD), X-ray photoelectron spectroscopy (XPS), Brunauer-Emmett-Teller (BET), and H_2 -temperature-programmed reduction (H_2 -TPR). The ESR was performed to investigate the effect of Sc_2O_3 doping. After that, we discussed the possible promotional effects of Sc_2O_3 on the ESR performance of the catalysts.

2. Results and Discussion

2.1. Catalyst Performance

The reactivity of ESR (data taken 24 h after the reaction started, similarly hereinafter) over a series of $\text{Co}_{1.25}\text{Zn}_1\text{Sc}_k$ (molar ratio) catalysts was optimized. The results (Figure 1) showed that CO_2 , CO, and CH_4 were the main carbon-containing products and the yield of ethyl ether was negligible. Under the reaction conditions of 0.5 MPa, 723 K, feed-gas composition of $\text{C}_2\text{H}_5\text{OH}/\text{H}_2\text{O}/\text{N}_2 = 15/45/40$ (molar ratio), and $\text{GHSV} = 150,000 \text{ mL}\cdot\text{h}^{-1}\cdot\text{g}_{\text{cat}}^{-1}$, the five catalysts $\text{Co}_{1.25}\text{Zn}_1\text{Sc}_k$ with varied k values at 0.2, 0.3, 0.4, 0.6, and 0.8 afforded $X(\text{EtOH})$ of 15.8%, 16.6%, 14.9%, 8.6%, and 5.6% with corresponding $\text{STY}(\text{H}_2)$ of 0.951, 1.037, 0.931, 0.668 and $0.513 \text{ mol}\cdot\text{h}^{-1}\cdot\text{g}_{\text{cat}}^{-1}$, respectively. It is clear that when the Sc/Zn molar ratio (k) was set at 0.3, the catalyst presented high $X(\text{EtOH})$ and $\text{STY}(\text{H}_2)$, and low $S(\text{CO})$ and $S(\text{CH}_4)$.

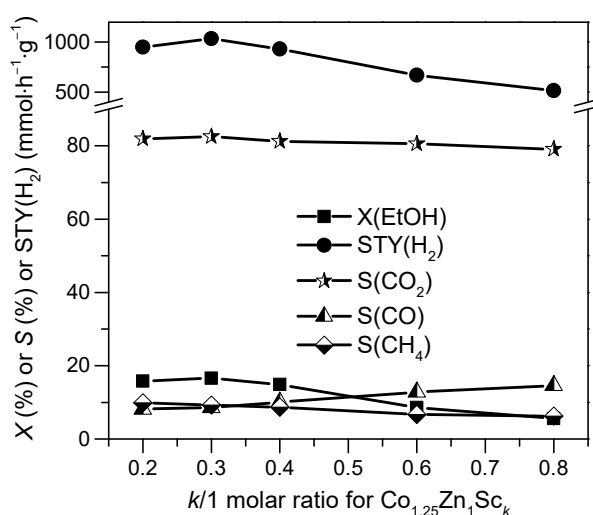


Figure 1. Performance of $\text{Co}_{1.25}\text{Zn}_1\text{Sc}_k$ catalyst for ethanol steam reforming (ESR) to H_2 as a function of Sc molar ratio. Reaction conditions: 0.5 MPa pressure, 723 K temperature, 15/45/40 molar ratio of $\text{EtOH}/\text{H}_2\text{O}/\text{N}_2$, and $150,000 \text{ mL}\cdot\text{h}^{-1}\cdot\text{g}_{\text{cat}}^{-1}$ GHSV.

Next, we investigated the Co/Zn molar ratio (i) effect on the reactivity of ESR. The results are showed in Figure 2. The four catalysts $\text{Co}_i\text{Zn}_1\text{Sc}_{0.3}$ with varied i values at 1.25, 2, 2.5, and 3

gave X(EtOH) of 16.6%, 19.1%, 18.5%, and 15.9% with corresponding STY(H₂) of 1.037, 1.151, 1.107 and 0.918 mol·h⁻¹·g_{cat}⁻¹, respectively, under the aforementioned reaction conditions. Obviously, the Co_iZn₁Sc_{0.3} catalyst with *i* = 2 could show high X(EtOH) and STY(H₂), and low S(CO) and S(CH₄).

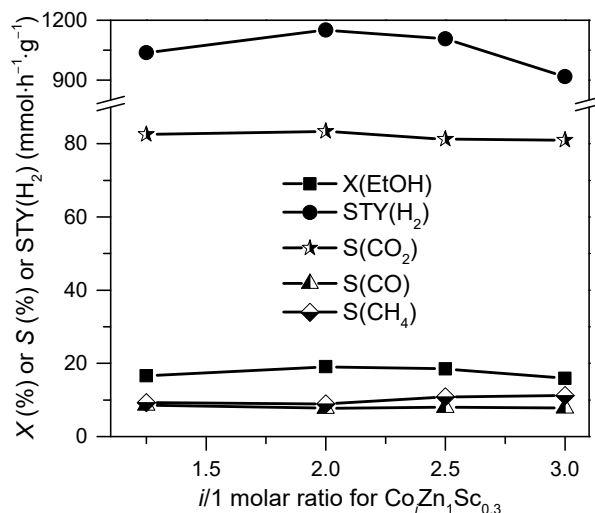


Figure 2. Performance of Co_iZn₁Sc_{0.3} catalyst for ESR to H₂ as a function of Co molar ratio. Reaction conditions: 0.5 MPa pressure, 723 K temperature, 15/45/40 molar ratio of EtOH/H₂O/N₂, and 150,000 mL·h⁻¹·g_{cat}⁻¹ GHSV.

The ESR performance of optimal Co₂Zn₁Sc_{0.3} catalyst was then evaluated under the aforementioned optimized reaction conditions: 0.5 MPa, 723 K, feed-gas composition EtOH/H₂O/N₂ = 15/45/40, and GHSV = 150,000 mL·h⁻¹·g_{cat}⁻¹. The results (data taken 100 h after the reaction started) showed that the X(EtOH) reached 16.6%, with S(CO₂), S(CO) and S(CH₄) of 80.6%, 7.9% and 11.5%, and the corresponding STY(H₂) of 1.099 mol·h⁻¹·g_{cat}⁻¹. This STY(H₂) value was 1.6 times that (0.684 mol·h⁻¹·g_{cat}⁻¹) of the Sc₂O₃-free counterpart Co₂Zn₁ under identical reaction conditions (Table 1). It has been reported that a 18.2% X(EtOH) was obtained over the Ni_{1.25}Zr₁Yb_{0.8} catalyst, affording 83.0% S(CO₂), 11.4% S(CO), and 5.6% S(CH₄) [20]. These values were slightly superior to those on the Co₂Zn₁Sc_{0.3} catalyst, but the STY(H₂) on Ni_{1.25}Zr₁Yb_{0.8} was much lower than that on Co₂Zn₁Sc_{0.3}. The catalyst containing noble metals such as RhFe/Ca-Al₂O₃ exhibited attracting X(EtOH). However, it gave the byproduct of S(CH₄) up to 39.7% [28]. More importantly, the STY(H₂) was far lower than the aforementioned catalysts. Generally speaking, the Co₂Zn₁Sc_{0.3} catalyst possessed the superior reactivity of ESR.

Table 1. Reactivity of ESR for H₂ production over Co₂Zn₁Sc_{0.3} and Co₂Zn₁ and the other compared catalysts.

Catalyst	S _{BET} (m ² ·g ⁻¹)	X-EtOH (%)	STY-H ₂ (mol·g ⁻¹ ·h ⁻¹)	Selectivity of C-Containing Products (%)			Reference
				CO ₂	CO	CH ₄	
Co ₂ Zn ₁ Sc _{0.3} ^a	134.2	16.6	1.099	80.6	7.9	11.5	This work
Co ₂ Zn ₁ ^a	61.7	10.8	0.684	73.5	8.1	18.4	
Ni _{1.25} Zr ₁ ^b	134.6	11.0	0.247	70.0	4.7	25.3	[20]
Ni _{1.25} Zr ₁ Yb _{0.8} ^b	161.8	18.2	0.396	83.0	11.4	5.6	
RhFe/Ca-Al ₂ O ₃ ^c	94.3	100	0.052	60.3	0.0	39.7	[28]

^a Reaction conditions: 0.5 MPa pressure, 723 K temperature, 15/45/40 molar ratio of EtOH/H₂O/N₂, and 150,000 mL·h⁻¹·g_{cat}⁻¹ GHSV. The activity data was taken 100 h after the reaction started; ^b Reaction conditions: 0.5 MPa pressure, 723 K temperature, 12.5/37.5/50 molar ratio of EtOH/H₂O/N₂, and 90,000 mL·h⁻¹·g_{cat}⁻¹ GHSV. The activity data was taken 100 h after the reaction started; ^c Reaction conditions: 623 K temperature, 1/10 molar ratio of EtOH/H₂O, and 34,000 mL·h⁻¹ GHSV. The activity data was taken 1.5 h after the reaction started.

Heat treatment at higher temperatures was performed to investigate the thermal resistance of Co_2Zn_1 and $\text{Co}_2\text{Zn}_1\text{Sc}_{0.3}$ catalysts. Typically, the thermal resistance of the catalyst was investigated under the reaction conditions of 0.5 MPa, $\text{EtOH}/\text{H}_2\text{O}/\text{N}_2 = 15/45/40$, $\text{GHSV} = 150,000 \text{ mL}\cdot\text{h}^{-1}\cdot\text{g}_{\text{-cat}}^{-1}$, and T ranging at 723–873 K. During the 90 h on stream, the catalysts were treated at high T at 823 and 873 K for 12 h, and then cooled down to 723 K for the ESR. The results are shown in Figure 3. To our surprise, the $X(\text{EtOH})$ fell to 0% over the Co_2Zn_1 catalyst. In contrast to this, the $X(\text{EtOH})$ on the catalyst $\text{Co}_2\text{Zn}_1\text{Sc}_{0.3}$ still maintained at a level of 12.6% after the whole process of heat treatment. The finding indicated that the catalyst $\text{Co}_2\text{Zn}_1\text{Sc}_{0.3}$ considerably improved the thermal resistance for ESR compared to the pristine Co-ZnO catalyst.

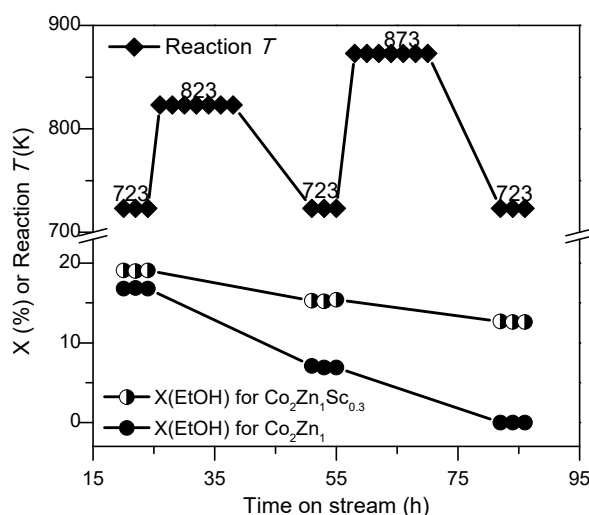


Figure 3. Thermal resistance of the catalysts $\text{Co}_2\text{Zn}_1\text{Sc}_{0.3}$ and Co_2Zn_1 for ESR as a function of time on stream at different temperatures. Reaction conditions: 0.5 MPa pressure, 723–873 K temperature, $150,000 \text{ mL}\cdot\text{h}^{-1}\cdot\text{g}_{\text{-cat}}^{-1}$ GHSV.

2.2. TEM Characterization

Figure 4 shows the TEM images and the corresponding particle distribution of as-reduced and spent catalysts of $\text{Co}_2\text{Zn}_1\text{Sc}_{0.3}$ and Co_2Zn_1 . The spent catalysts were run through the ESR for 24 h under the reaction conditions of 0.5 MPa, 823 K, feed-gas composition of $\text{C}_2\text{H}_5\text{OH}/\text{H}_2\text{O}/\text{N}_2 = 15/45/40$, and $\text{GHSV} = 150,000 \text{ mL}\cdot\text{h}^{-1}\cdot\text{g}_{\text{-cat}}^{-1}$. It can be seen that the $\text{Co}_2\text{Zn}_1\text{Sc}_{0.3}$ catalyst exhibited excellent dispersion, with a wide size distribution from 8 to 20 nm and a mean size of 13.5 nm. For the reduced Co_2Zn_1 catalyst, the particle size ranged between 9 nm and 30 nm, with a mean size of 17.2 nm. It could be deduced that introducing the Sc_2O_3 to Co-ZnO catalyst was in favor of boosting the dispersion of the active species. On the spent $\text{Co}_2\text{Zn}_1\text{Sc}_{0.3}$ catalyst, the observed nanoparticles were fairly uniform in shape and size. The particle size was estimated to be in the range of 12–28 nm, with a mean size of 19.1 nm. In contrast, the particle size of the spent Co_2Zn_1 catalyst was in the range of 20–75 nm, accompanied with the formation of an appreciable amount of carbon-nanotubes or carbon-nanofibers. It could be concluded that the addition of Sc_2O_3 to Co-ZnO inhibited the growth of the particles to some extent, and thus effectively suppressed the sintering and deactivation of the catalyst. These results were in line with the surface area values of the two spent catalysts, as well as the ESR reactivity over the two catalysts (Table 1 and Figure 3).

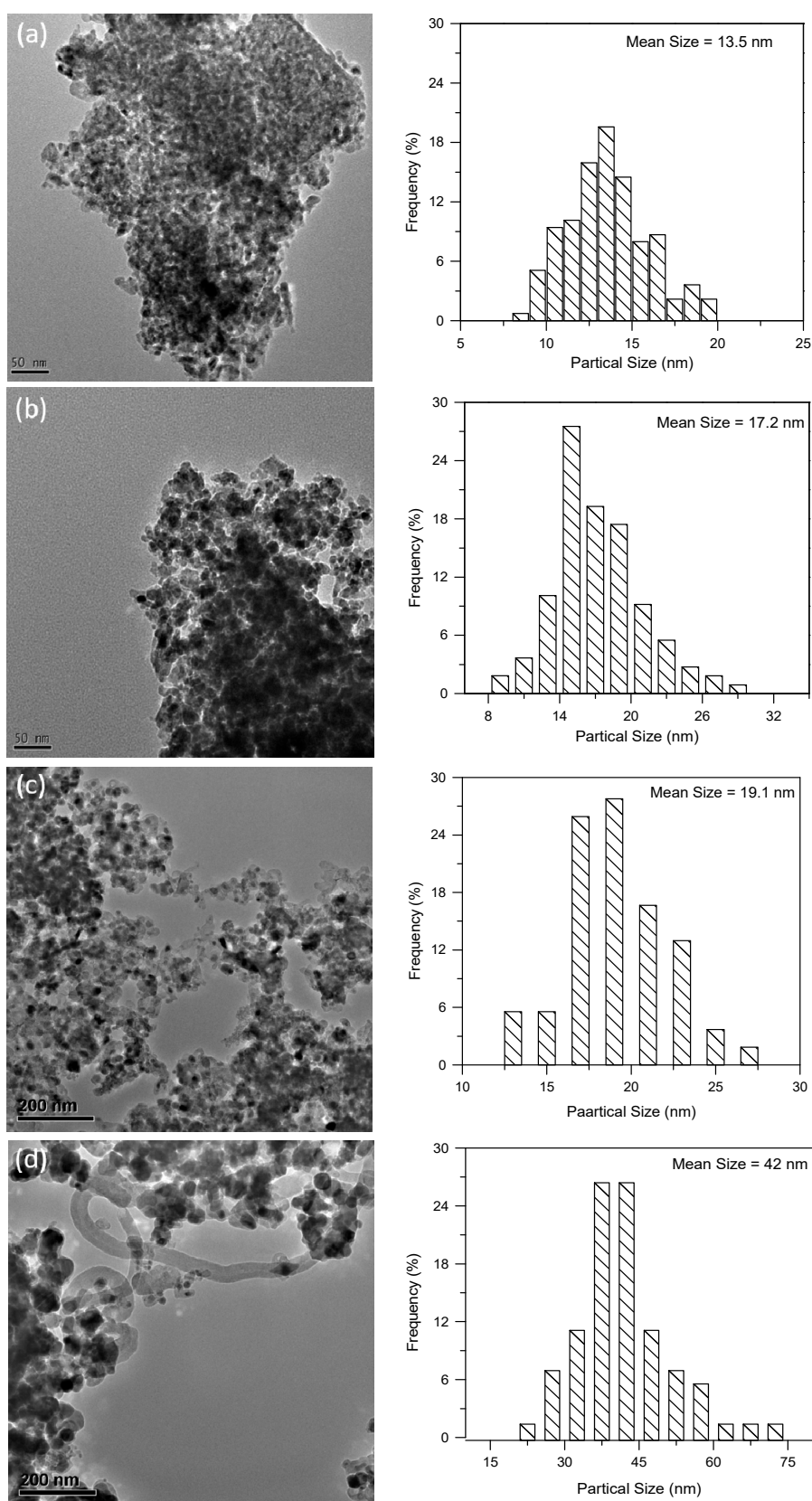


Figure 4. TEM images of as-reduced catalysts (a) $\text{Co}_2\text{Zn}_1\text{Sc}_{0.3}$ and (b) Co_2Zn_1 , and the spent catalysts (c) $\text{Co}_2\text{Zn}_1\text{Sc}_{0.3}$ and (d) Co_2Zn_1 .

2.3. XRD and XPS Characterization

The XRD patterns, which are used to identify the phase structure and crystallite size of the materials of the reduced and spent catalysts of Co_2Zn_1 and Co-ZnO doped with Sc_2O_3 , are shown in Figure 5. No matter whether the samples were reduced or spent, pure Co-ZnO catalyst or doped with Sc_2O_3 , the characteristic diffraction of the ZnO appeared at $2\theta = 31.7^\circ, 34.4^\circ, 36.2^\circ, 47.5^\circ, 56.5^\circ, 62.8^\circ,$ and 67.9° in all the samples. Except for several characteristic diffraction peaks corresponding to ZnO , the peaks located at $2\theta = 44.2^\circ, 51.5^\circ$ and $2\theta = 36.8^\circ, 59.4^\circ, 65.2^\circ$ were ascribed to metallic Co and Co_3O_4 for the reduced Co_2Zn_1 catalyst, respectively. As for the $\text{Co}_2\text{Zn}_1\text{Sc}_{0.3}$ catalyst, the main Co species are in the form of CoO with the diffraction lines at $2\theta = 42.4^\circ$ and 61.5° . The results indicated that the Sc_2O_3 -doping had a positive effect on the crystal phase of Co-ZnO catalyst, which would be favorable to stabilize Co^{n+} ($n = 1$ or 2) with high oxidation states, thus effectively refraining from sintering. On the other hand, the XRD patterns of the spent catalysts were similar to those of as-reduced ones, except for the sharper peak shape. The Co and Zn components existed mainly in the forms of metallic Co and ZnO for the catalysts after reaction. The particle size of Co and ZnO in the two spent catalysts was estimated according to the Scherrer's equation. The average particle sizes of Co and ZnO were 3.5 and 26.9 nm for $\text{Co}_2\text{Zn}_1\text{Sc}_{0.3}$, and 19.6 and 37.2 nm for Co_2Zn_1 , respectively. The results showed a significant effect on the dispersion of Co species with the addition of small amounts of Sc_2O_3 .

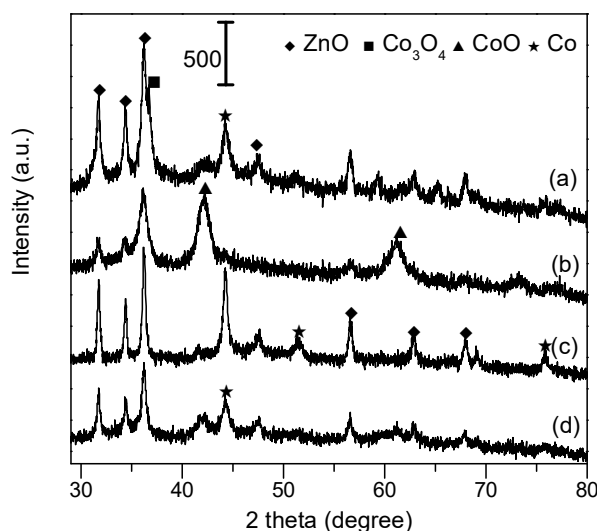


Figure 5. XRD patterns of the reduced catalysts of (a) Co_2Zn_1 , (b) $\text{Co}_2\text{Zn}_1\text{Sc}_{0.3}$, and the spent catalysts of (c) Co_2Zn_1 ; (d) $\text{Co}_2\text{Zn}_1\text{Sc}_{0.3}$.

XPS analysis is a powerful way of distinguishing the chemical environment and the change in content of surface species. The XPS profile of the spent catalysts displayed that the signals assigned to the Co , Zn , Sc , and O atoms were observed on the surface of the Sc_2O_3 -containing and Sc_2O_3 -free catalysts. In the $\text{Co } 2p$ XPS profile (Figure 6A) of the Sc_2O_3 -doped Co-ZnO catalyst, the main peak shifted to a lower binding energy compared with the Sc_2O_3 -free counterpart. A similar situation was happened on the $\text{Zn } 2p$ XPS profile (Figure 6B). These findings implied that the electronic density on Co atoms increased after Sc_2O_3 doping [29,30], which was in favor of the adsorption and activation of the reactants or intermediates [31–33]. Sc species in the Sc_2O_3 -doped Co-ZnO catalysts existed in the form of Sc_2O_3 based on the $\text{Sc } 2p$ XPS profile (Figure 6C).

Figure 6A displays the $\text{Co } 2p$ XPS profile taken on the used catalysts of $\text{Co}_2\text{Zn}_1\text{Sc}_{0.3}$ and Co_2Zn_1 . It displays a main line and a satellite for $\text{Co } 2p$ XPS profile. The observed $\text{Co}(2p_{3/2})$ and $\text{Co}(2p_{1/2})$ peaks appeared at about 780.9 eV and 796.6 eV, respectively. According to the literature [34], the $\text{Co } 2p$ XPS profile could be divided into three peaks. They were Co_x^0 , CoO and $\text{Co}(\text{OH})_2$ with the corresponding $\text{Co}^{n+}(2p_{3/2})$ B.E. values at 778.0 eV, 780.4 eV and 782.0 eV, respectively [35–37]. The binding energies

of $\text{Co}^{n+}(2p_{3/2})$ for the reference compounds, along with their relative intensities, are given in Table 2. From the above analysis, it could be concluded that the doping of small amounts of Sc_2O_3 into the Co_2Zn_1 catalyst led to lessening significantly the mol % of Co^0 species (Figure 6A and Table 2). This is in agreement with the XRD results shown in Figure 5.

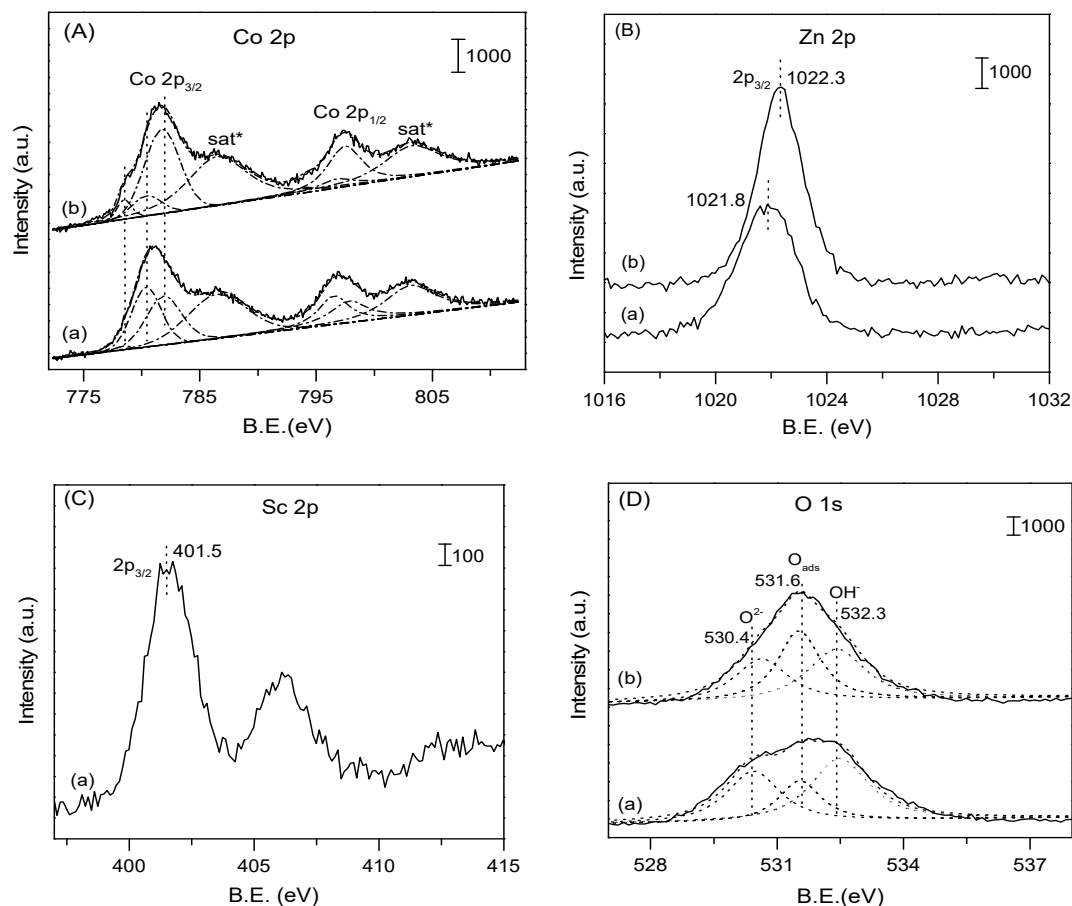


Figure 6. X-ray photoelectron spectroscopy (XPS) profiles for the spent catalysts of (a) $\text{Co}_2\text{Zn}_1\text{Sc}_{0.3}$ and (b) Co_2Zn_1 ; (A) Co 2p; (B) Zn 2p; (C) Sc 2p; (D) O 1s.

Table 2. XPS binding energy and relative content of the Co species with different valence states at the surface of the tested catalysts.

Catalyst	B.E. (Co $2p_{3/2}$)/eV			Relative Content/mol %		
	Co^0	CoO	$\text{Co}(\text{OH})_2$	Co^0	CoO	$\text{Co}(\text{OH})_2$
Co_2Zn_1	778.5	780.4	781.8	7.7	15.5	76.8
$\text{Co}_2\text{Zn}_1\text{Sc}_{0.3}$	778.4	780.4	781.9	1.2	48.2	50.6

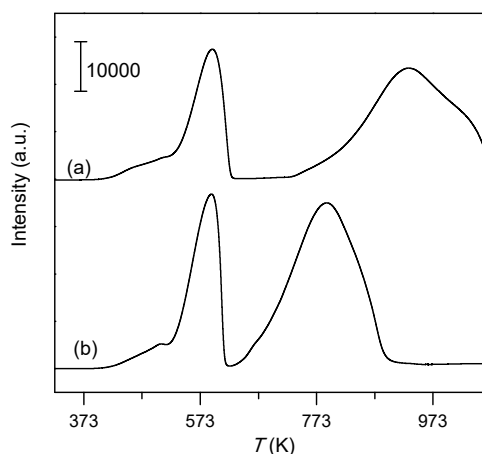
As seen in the O 1s XPS profile depicted in Figure 6D, the peaks located at 530.4 eV, 531.6 eV and 532.3 eV were ascribed to oxide anion (O^{2-}), adsorbed oxygen (O_{ads}) and hydroxide anion (OH^-), successively, on the surface of the spent catalysts of $\text{Co}_2\text{Zn}_1\text{Sc}_{0.3}$ and Co_2Zn_1 [31,38]. The content of the O species was calculated and presented in Table 3. The mol % of O^{2-} and OH^- species arrived 33.9% and 44.6% on the surface of $\text{Co}_2\text{Zn}_1\text{Sc}_{0.3}$ respectively, being 1.22 and 1.44 times of the corresponding values (27.6% and 35.9%) of the compared Co_2Zn_1 catalyst. However, the content of O_{ads} (21.5%) on the surface of the spent $\text{Co}_2\text{Zn}_1\text{Sc}_{0.3}$ was evidently lower than the corresponding values (36.5%) of the compared Co_2Zn_1 catalyst. These results indicated that O^{2-} and OH^- species favored the H_2 production based on our experimental results, which needs further research in the future.

Table 3. XPS binding energy and relative content of the O-species with different valence states at the surface of the catalysts.

Catalyst	B.E. (Co 2p _{3/2})/eV			Relative Content/mol %		
	O ²⁻	O _{ads}	OH ⁻	O ²⁻	O _{ads}	OH ⁻
Co ₂ Zn ₁	530.6	531.5	532.4	27.6	36.5	35.9
Co ₂ Zn ₁ Sc _{0.3}	530.5	531.6	532.5	33.9	21.5	44.6

2.4. H₂-TPR

The H₂-TPR profiles of Co₂Zn₁Sc_{0.3} and Co₂Zn₁ catalysts are illustrated in Figure 7. The H₂-TPR curve of Co₂Zn₁ catalyst (Figure 7b) showed the two peaks at 593 K and 791 K, successively. The former may be due to the reduction of Co₂O₃ to Co₃O₄, or further to CoO. The latter is likely attributed to the reduction of Co₃O₄ or CoO to Co⁰ [39,40], which interacted strongly with ZnO surface, and, thus, were difficult to be reduced at lower temperatures. The addition of the appropriate amount of Sc₂O₃ to the Co₂Zn₁ host further strengthened the interaction between Coⁿ⁺ species and the Zn_x-Sc_y-O_z compound-oxide surface, leading to an elevating reduction-temperature of those Coⁿ⁺ species (with the main TPR peak elevating to 933 K from 791 K) (Figure 7a), and stabilizing and anchoring Coⁿ⁺ particles. This result was in line with the aforementioned results of XPS observation and the thermal stability test of the catalysts.

**Figure 7.** H₂-temperature-programmed reduction (H₂-TPR) profiles of the oxide catalysts: (a) Co₂Zn₁Sc_{0.3}; (b) Co₂Zn₁.

3. Discussion

It is well known that most of the catalyst deactivation of ESR is attributed to the active metal sintering and the deposition of various type of carbon on the surface of the catalyst [41,42]. How to solve these problems is the main challenge in this field. In this work, we apply the ion-doped method to the catalyst preparation. Based on the ionic radius of Sc³⁺ and Zn²⁺ being similar to each other, Sc³⁺ could easily enter into the ZnO lattice. Schottky defects in the form of cationic vacancies would be generated simultaneously for reaching charge compensation. Hence, Coⁿ⁺ can be immobilized at the surface cation-sites. This result is in accordance with the former work of our teams [43]. This will be conducive to suppressing the agglomeration of the Coⁿ⁺ species and maintaining the high Coⁿ⁺ dispersion between the metal Co and ZnO though electronic effect, thus markedly improving the activity and thermal durability of the catalyst. The transformation of O species was also responsible for the excellent catalytic performance, which needs in-depth discussion. These points are proved by the results of the characterizations, and all of the above factors will be responsible for the enhancement effect of the Sc₂O₃ introduction.

4. Experimental

4.1. Catalyst Preparation

The catalysts Co-ZnO and Sc₂O₃-doped Co-ZnO were prepared by a co-precipitation method. Typically, an appropriate amount of Co(NO₃)₂·6H₂O and Zn(NO₃)₂·6H₂O (Sinopharm Chemical Reagent Co. Ltd., Shanghai, China), and Sc(NO₃)₃·6H₂O (Diyang Chemical Reagent Co. Ltd., Shanghai, China) were dissolved in deionized water together. The required amount of K₂CO₃ (Sinopharm Chemical Reagent Co. Ltd., Shanghai, China) was made to aqueous solution in a beak and put it into a water bath at 353 K. The former solution was rapidly added into the latter until the pH ≈ 7 was achieved. The suspension was continuously stirred for another 30 min and then filtered. The precipitate was washed five times, then dried at 383 K for 12 h and calcined in a muffle oven at 623 K for 2 h. Co-ZnO was prepared in a similar way. All samples were pressed, crushed, and sieved to a size of 20–40 mesh for the activity testing.

4.2. Catalytic Evaluation

ESR reactions were tested in a fixed-bed continuous-flow reactor combined with gas chromatograph (GC). The catalyst was reduced at 623 K for 5 h under purified H₂ stream. The ESR reaction was performed under the reaction condition of 0.5 MPa, 723 K, and a feed gas composition of C₂H₅OH/H₂O/N₂ = 15/45/40 (molar ratio) (Sinopharm Chemical Reagent Co. Ltd., Shanghai, China), and GHSV = 150,000 mL·h⁻¹·g_{cat}⁻¹. The feed contained C₂H₅OH, and H₂O was introduced into the reactor by a syringe pump (Series II Pump, 10 mL Heads) with N₂ as the internal standard and dilution gas. The C₂H₅OH and H₂O mixed liquid was vaporized at 473 K before access to the reactor.

Prior to entering the sampling valve of the GC, the products passed through a low constant temperature bath (DC-2006) to separate liquid products. An online GC (GC-2014C, Shimadzu, Kyoto, Japan), equipped with a thermal conductivity detector (TCD) (TDX-01 column) and with He as carrier gas, was used to separate N₂, CO, CH₄ and CO₂. H₂ was detected online by TCD using another GC-2014C (TDX-01 column) and with Ar as carrier gas.

Analysis of the liquid products showed that ethyl ether could be ignored and CO₂, CO, and CH₄ were the main products. Thus, ethanol conversion (symbolized as X(EtOH)) (Equation (1)), selectivity of CO₂, CO, and CH₄ (symbolized as S(CO₂), S(CO), and S(CH₄)) (Equations (2)–(4)), and H₂ space-time-yield (symbolized as STY(H₂)) (Equation (5)) could be calculated through a N₂-internal standard method according to the following equations:

$$X_{\text{CH}_3\text{CH}_2\text{OH}} = \frac{n_{\text{CO}_2} + n_{\text{CO}} + n_{\text{CH}_4}}{2n_{\text{CH}_3\text{CH}_2\text{OH}}^{\text{in}}} = \frac{F_{\text{N}_2}f'_{\text{CO}_2}A_{\text{CO}_2} + F_{\text{N}_2}f'_{\text{CO}}A_{\text{CO}} + F_{\text{N}_2}f'_{\text{CH}_4}A_{\text{CH}_4}}{44800A_{\text{N}_2}n_{\text{CH}_3\text{CH}_2\text{OH}}^{\text{in}}} \quad (1)$$

$$S_{\text{CO}_2} = \frac{f'_{\text{CO}_2}A_{\text{CO}_2}}{f'_{\text{CO}_2}A_{\text{CO}_2} + f'_{\text{CO}}A_{\text{CO}} + f'_{\text{CH}_4}A_{\text{CH}_4}} \quad (2)$$

$$S_{\text{CO}} = \frac{f'_{\text{CO}}A_{\text{CO}}}{f'_{\text{CO}_2}A_{\text{CO}_2} + f'_{\text{CO}}A_{\text{CO}} + f'_{\text{CH}_4}A_{\text{CH}_4}} \quad (3)$$

$$S_{\text{CH}_4} = \frac{f'_{\text{CH}_4}A_{\text{CH}_4}}{f'_{\text{CO}_2}A_{\text{CO}_2} + f'_{\text{CO}}A_{\text{CO}} + f'_{\text{CH}_4}A_{\text{CH}_4}} \quad (4)$$

$$\text{STY}_{\text{H}_2} = \frac{n_{\text{H}_2}}{m_{\text{cat.}}} = \frac{60F_{\text{N}_2}f'_{\text{H}_2}A_{\text{H}_2}}{22400A_{\text{N}_2}m_{\text{cat.}}} \quad (5)$$

where, F_{N_2} represents the flow of N₂ (mL·min⁻¹), $n_{\text{CH}_3\text{CH}_2\text{OH}}^{\text{in}}$ represents the molar of liquid feed (ethanol and H₂O) inputting to the reactor, n represents the molar of the production (such as CO, CO₂,

CH₄, etc.), f' represents the molar calibration factor, A represents the peak area in GC; m_{cat} represents the catalyst weight loaded.

4.3. Characterizations

Transmission electron microscopy (TEM) measurements were performed on the Technai F30 and F20 electron microscope (FEI Corp., Hillsboro, OR, USA). XRD measurements were carried out on an X'Pert PRO X-ray diffractometer (Ultima IV, Rigaku, Tokyo, Japan) with Cu K α ($\lambda_{\alpha 1} = 0.15406$ nm, $\lambda_{\alpha 2} = 0.15443$ nm) radiation. X-ray photoelectron spectroscopy (PHI Quantum 2000 Scanning ESCA Microprobe, PHI, Eden Prairie, MN, USA) measurements were done on a VG ESCA LAB MK-2 apparatus with Al-K α radiation (15 kV, 25 W, $h\nu = 1486.6$ eV) under ultrahigh vacuum (10^{-7} Pa), calibrated internally by the carbon deposit C(1s) ($E_b = 284.6$ eV). The specific surface area was determined by N₂ adsorption using a Micromeritics ASAP 2020 system (Micromeritics, Norcross, GA, USA). Tests of H₂-temperature-programmed reduction (H₂-TPR) and H₂-temperature-programmed desorption (H₂-TPD) of the catalysts were conducted on a fixed-bed continuous-flow microreactor, and change of hydrogen-signal was monitored by an on-line GC (Shimadzu GC-8A, Kyoto, Japan) with a TCD.

5. Conclusions

Sc₂O₃-doped Co-ZnO catalyst for H₂ production by ESR was prepared. The optimized Co₂Zn₁Sc_{0.3} exhibited the highest EtOH conversion and STY of H₂. The H₂ STY was 1.099 mol·h⁻¹·g_{cat}⁻¹, 1.6 times higher than that on the Co-ZnO catalyst without Sc₂O₃ doping under the optimal reaction conditions. XPS and TPR results disclosed that the electronic interaction between Co and ZnO after Sc₂O₃ addition was strengthened, which was beneficial to the dispersion of the Coⁿ⁺. The introduction of Sc₂O₃ to Co-ZnO also promoted the formation of O²⁻ and OH⁻, which would be conducive to H₂ production, but it needs the further investigation. The present work may contribute to the precise design of catalysts for ESR to produce H₂ with desirable activity and better durability.

It must be admitted that the improved performance has been achieved over the present Sc₂O₃-doped Co-ZnO catalyst, but the selectivity to CO and CH₄ is still high, especially when the ESR is run at the reaction temperature higher than 723 K. It is well known that CO is poison to the anode of the fuel cell and the formation of CH₄ sacrifices the selectivity of H₂. Therefore, more efforts are necessary to fabricate novel catalysts that can efficiently generate more H₂ and minimize CO selectivity. In particular, we must consider the catalysts that minimize undesirable products at higher temperature operations in future work.

Acknowledgments: This work was supported by the Natural Science Foundation of China (21473145 and 91545115), and the Program for Innovative Research Team in Chinese Universities (No. IRT_14R31).

Author Contributions: Hongbin Zhang conceived and designed the experiments; Xuelian Liang performed the experiments; Xinping Shi and Fanfan Zhang analyzed the data; Yuyang Li contributed reagents/materials/analysis tools; Xuelian Liang and Youzhu Yuan wrote the paper.

Conflicts of Interest: The authors declare no conflict of interest. The founding sponsors had no role in the design of the study; in the collection, analyses, or interpretation of data; in the writing of the manuscript, and in the decision to publish the results.

References

1. Mattos, L.V.; Jacobs, G.; Davis, B.H.; Noronha, F.B. Production of hydrogen from ethanol: Review of reaction mechanism and catalyst deactivation. *Chem. Rev.* **2012**, *112*, 4094–4123. [[CrossRef](#)] [[PubMed](#)]
2. Ni, M.; Leung, D.Y.C.; Leung, M.K.H. A review on reforming bio-ethanol for hydrogen production. *Int. J. Hydrogen Energy* **2007**, *32*, 3238–3247. [[CrossRef](#)]
3. Breen, J.P.; Burch, R.; Coleman, H.M. Metal-catalysed steam reforming of ethanol in the production of hydrogen for fuel cell applications. *Appl. Catal. B Environ.* **2002**, *39*, 65–74. [[CrossRef](#)]

4. Auprêtre, F.; Descorme, C.; Duprez, D. Bio-ethanol catalytic steam reforming over supported metal catalysts. *Catal. Commun.* **2002**, *3*, 263–267. [[CrossRef](#)]
5. Kugai, J.; Subramani, V.; Song, C.; Engelhard, M.H.; Chin, Y.H. Effects of nanocrystalline CeO₂ supports on the properties and performance of Ni-Rh bimetallic catalyst for oxidative steam reforming of ethanol. *J. Catal.* **2006**, *238*, 430–440. [[CrossRef](#)]
6. Cai, W.; Wang, F.; Zhan, E.; Van Veen, A.C.; Mirodatos, C.; Shen, W. Hydrogen production from ethanol over Ir/CeO₂ catalysts: A comparative study of steam reforming, partial oxidation and oxidative steam reforming. *J. Catal.* **2008**, *257*, 96–107. [[CrossRef](#)]
7. De Lima, S.M.; Silva, A.M.; Graham, U.M.; Jacobs, G.; Davis, B.H.; Mattos, L.V.; Noronha, F.B. Ethanol decomposition and steam reforming of ethanol over CeZrO₂ and Pt/CeZrO₂ catalyst: Reaction mechanism and deactivation. *Appl. Catal. A Gen.* **2009**, *352*, 95–113. [[CrossRef](#)]
8. Llorca, J.; Piscina, P.R.; Dalmon, J.A.; Sales, J.; Homs, N. CO-free hydrogen from steam reforming of bioethanol over ZnO-supported cobalt catalysts: Effect of the metallic precursor. *Appl. Catal. B Environ.* **2003**, *43*, 355–369. [[CrossRef](#)]
9. Llorca, J.; Homs, N.; Sales, J.; Fierro, J.L.; Piscina, P.R. Effect of sodium addition on the performance of Co-ZnO-based catalysts for hydrogen production from bioethanol. *J. Catal.* **2004**, *222*, 470–480. [[CrossRef](#)]
10. Batista, M.S.; Santos, R.K.S.; Assaf, E.M.; Assaf, J.M.; Ticianelli, E.A. Characterization of the activity and stability of supported cobalt catalysts for the steam reforming of ethanol. *J. Power Sources* **2003**, *124*, 99–103. [[CrossRef](#)]
11. Song, H.; Zhang, L.; Watson, R.B.; Braden, D.; Ozkan, U.S. Investigation of bio-ethanol steam reforming over cobalt-based catalysts. *Catal. Today* **2007**, *129*, 346–354. [[CrossRef](#)]
12. Song, H.; Ozkan, U.S. Ethanol steam reforming over Co-based catalysts: Role of oxygen mobility. *J. Catal.* **2009**, *261*, 66–74. [[CrossRef](#)]
13. De Lima, S.M.; da Silva, A.M.; da Costa, L.O.O.; Graham, U.M.; Jacobs, G.; Davis, B.H.; Mattos, L.V.; Noronha, F.B. Study of catalyst deactivation and reaction mechanism of steam reforming, partial oxidation, and oxidative steam reforming of ethanol over Co/CeO₂ catalyst. *J. Catal.* **2009**, *268*, 268–281. [[CrossRef](#)]
14. Chiou, J.Y.Z.; Wang, W.Y.; Yang, S.Y.; Lai, C.L.; Huang, H.H.; Wang, C.B. Ethanol steam reforming to produce hydrogen over Co/ZnO and PtCo/ZnO catalysts. *Catal. Lett.* **2013**, *143*, 501–507. [[CrossRef](#)]
15. Bellido, J.D.A.; Assaf, E.M. Nickel catalysts supported on ZrO₂, Y₂O₃-stabilized ZrO₂ and CaO-stabilized ZrO₂ for the steam reforming of ethanol: Effect of the support and nickel load. *J. Power Sources* **2008**, *177*, 24–32. [[CrossRef](#)]
16. Rossetti, I.; Biffi, C.; Bianchi, C.L.; Nichele, V.; Signoretto, M.; Menegazzo, F.; Finocchio, E.; Ramis, G.; Di Michele, A. Ni/SiO₂ and Ni/ZrO₂ catalysts for the steam reforming of ethanol. *Appl. Catal. B Environ.* **2012**, *117–118*, 384–396. [[CrossRef](#)]
17. Akiyama, M.; Oki, Y.; Nagai, M. Steam reforming of ethanol over carburized alkali-doped nickel on zirconia and various supports for hydrogen production. *Catal. Today* **2012**, *181*, 4–13. [[CrossRef](#)]
18. Coleman, L.J.I.; Epling, W.; Hudgins, R.R.; Croiset, E. Ni/Mg-Al mixed oxide catalyst for the steam reforming of ethanol. *Appl. Catal. A Gen.* **2009**, *363*, 52–63. [[CrossRef](#)]
19. Galetti, A.E.; Barroso, M.N.; Gomez, M.F.; Arrua, L.A.; Monzón, A.; Abello, M.C. Promotion of Ni/MgAl₂O₄ catalysts with rare earths for the ethanol steam reforming reaction. *Catal. Lett.* **2012**, *142*, 1461–1469. [[CrossRef](#)]
20. Hou, J.; Liu, Z.M.; Lin, G.D.; Zhang, H.B. Novel Ni-ZrO₂ catalyst doped with Yb₂O₃ for ethanol steam reforming. *Int. J. Hydrogen Energy* **2014**, *39*, 1315–1324. [[CrossRef](#)]
21. Lin, J.Y.; Chen, L.W.; Choong, C.K.S.; Zhong, Z.Y.; Huang, L. Molecular catalysis for the steam reforming of ethanol. *Sci. China Chem.* **2015**, *58*, 60–78. [[CrossRef](#)]
22. Vargas, J.C.; Libs, S.; Roger, A.C.; Kiennemann, A. Study of Ce-Zr-Co fluorite-type oxide as catalysts for hydrogen production by steam reforming of bioethanol. *Catal. Today* **2005**, *107–108*, 417–425. [[CrossRef](#)]
23. Erdőhelyi, A.; Raskó, J.; Kecskés, T.; Tóth, M.; Dömök, M.; Baán, K. Hydrogen formation in ethanol reforming on supported noble metal catalysts. *Catal. Today* **2006**, *116*, 367–376. [[CrossRef](#)]
24. Frusteri, F.; Freni, S.; Chiodo, V.; Donato, S.; Bonura, G.; Cavallaro, S. Steam and auto-thermal reforming of bio-ethanol over MgO and CeO₂ Ni supported catalysts. *Int. J. Hydrogen Energy* **2006**, *31*, 2193–2199. [[CrossRef](#)]

25. Romero-Sarria, F.; Vargas, J.C.; Roger, A.; Kiennemann, A. Hydrogen production by steam reforming of ethanol: Study of mixed oxide catalysts $\text{Ce}_2\text{Zr}_{1.5}\text{Me}_{0.5}\text{O}_8$: Comparison of Ni/Co and effect of Rh. *Catal. Today* **2008**, *133*, 149–153. [CrossRef]
26. Galetti, A.E.; Gomez, M.F.; Arrua, L.A.; Marchi, A.J.; Abello, M.C. Study of CuCoZnAl oxide as catalyst for the hydrogen production from ethanol reforming. *Catal. Commun.* **2008**, *9*, 1201–1208. [CrossRef]
27. Wang, H.; Liu, Y.; Wang, L.; Qin, Y.N. Study on the carbon deposition in steam reforming of ethanol over Co/CeO₂ catalyst. *Chem. Eng. J.* **2008**, *145*, 25–31. [CrossRef]
28. Choong, C.K.S.; Chen, L.W.; Du, Y.H.; Schreyer, M.; Daniel Ong, S.W.; Poh, C.K.; Hong, L.; Borgna, A. The role of metal-support interaction for CO-free hydrogen from low temperature ethanol steam reforming on Rh-Fe catalysts. *Phys. Chem. Chem. Phys.* **2017**, *19*, 4199–4207. [CrossRef] [PubMed]
29. Yu, J.; Mao, D.S.; Ding, D.; Guo, X.M.; Lu, G.Z. New insights into the effects of Mn and Li on the mechanistic pathway for CO hydrogenation on Rh-Mn-Li/SiO₂ catalysts. *J. Mol. Catal. A Chem.* **2016**, *423*, 151–159. [CrossRef]
30. Qin, Z.Z.; Zhou, X.H.; Su, M.T.; Jiang, Y.X.; Ji, H.B. Hydrogenation of CO₂ to dimethyl ether on La-, Ce-modified Cu-Fe/HZSM-5 catalysts. *Catal. Commun.* **2016**, *75*, 78–82. [CrossRef]
31. Lu, J.Z.; Yang, L.J.; Xu, B.L.; Wu, Q.; Zhang, D.; Yuan, S.J.; Zhai, Y.; Wang, X.; Fan, Y.; Hu, Z. Promotion effects of nitrogen doping into carbon nanotubes on supported iron Fischer-Tropsch catalysts for lower olefins. *ACS Catal.* **2014**, *4*, 613–621. [CrossRef]
32. Zhou, J.F.; Duan, X.P.; Ye, L.M.; Zheng, J.W.; Li, M.M.J.; Tsang, S.E.; Yuan, Y.Z. Enhanced chemoselective hydrogenation of dimethyl oxalate to methyl glycolate over bimetallic Ag-Ni/SBA-15 catalysts. *Appl. Catal. A Gen.* **2015**, *505*, 344–353. [CrossRef]
33. Huang, Y.; Ariga, H.; Zheng, X.L.; Duan, X.P.; Takakusagi, S.; Asakura, K.; Yuan, Y.Z. Silver-modulated SiO₂-supported copper catalysts for selective hydrogenation of dimethyl oxalate to ethylene glycol. *J. Catal.* **2013**, *307*, 74–83. [CrossRef]
34. Moulder, J.F.; Stickle, W.F.; Sobol, P.E.; Bomben, K.D. *Handbook of X-ray Photoelectron Spectroscopy—A Reference Book of Standard Spectra for Identification and Interpretation of XPS Data*; Physical Electronics Inc.: Eden Prairie, MN, USA, 1995.
35. Ernst, B.; Libs, S.; Chaumette, P.; Kiennemann, A. Preparation and characterization of Fischer-Tropsch active Co/SiO₂ catalysts. *Appl. Catal. A Gen.* **1999**, *186*, 145–168. [CrossRef]
36. Venezia, A.M.; La Parola, V.; Liotta, L.F.; Pantaleo, G.; Lualdi, M.; Boutonnet, M.; Jaras, S. Co/SiO₂ catalysts for Fischer-Tropsch synthesis; effect of Co loading and support modification by TiO₂. *Catal. Today* **2012**, *197*, 18–23. [CrossRef]
37. Dong, X.; Liang, X.L.; Li, H.Y.; Lin, G.D.; Zhang, P.; Zhang, H.B. Preparation and characterization of carbon nanotube-promoted Co-Cu catalyst for higher alcohol synthesis from syngas. *Catal. Today* **2009**, *147*, 158–165. [CrossRef]
38. Wang, X.; Jiang, Z.Y.; Zheng, B.J.; Xie, Z.X.; Zheng, L.S. Synthesis and shape-dependent catalytic properties of CeO₂ nanocubes and truncated octahedra. *CrystEngComm* **2012**, *14*, 7579–7582. [CrossRef]
39. Sun, Y.F.; Li, J.H.; Wang, M.N.; Hua, B.; Li, J.; Luo, J.L. A-site deficient chromite perovskite with in situ exsolution of nano-Fe: A promising bi-functional catalyst bridging the growth of CNTs and SOFCs. *J. Mater. Chem. A* **2015**, *3*, 14625–14630. [CrossRef]
40. Ogo, S.; Shimizu, T.; Nakazawa, Y.; Mukawa, K.; Mukai, D.; Sekine, Y. Steam reforming of ethanol over K promoted Co catalyst. *Appl. Catal. A Gen.* **2015**, *495*, 30–38. [CrossRef]
41. Wu, C.F.; Dupont, V.; Nahil, M.A.; Dou, B.L.; Chen, H.S.; Williams, P.T. Investigation of Ni/SiO₂ catalysts prepared at different conditions for hydrogen production from ethanol steam reforming. *J. Energy Inst.* **2017**, *90*, 276–284. [CrossRef]
42. Compagnoni, M.; Tripodi, A.; Rossetti, L. Parametric study and kinetic testing for ethanol steam reforming. *Appl. Catal. B Environ.* **2017**, *203*, 899–909. [CrossRef]
43. Yang, L.; Lin, G.D.; Zhang, H.B. Highly efficient Pd-ZnO catalyst doubly promoted by CNTs and Sc₂O₃ for methanol steam reforming. *Appl. Catal. A Gen.* **2013**, *455*, 137–144. [CrossRef]

